

Advanced cardiovascular disease classification using multi-modal imaging and deep learning

Benila Christabel Thankappan, Thanammal Kakkumperumal Krishnammal

Department of Computer Science and Research Centre, S. T. Hindu College, Nagercoil-629002, Affiliated to Manonmaniam Sundaranar University, Abishekapatti, Tirunelveli-627012, Tamilnadu, India

Article Info

Article history:

Received Aug 2, 2024

Revised Dec 16, 2024

Accepted Dec 27, 2024

Keywords:

Cardiovascular disease

Deep learning

Dilated convolutional neural network

Grey level co-occurrence matrix

Multi-model images

Wavelet transformer based multiscale Retinex

ABSTRACT

Cardiovascular disease (CVD) is a disorder of the heart and blood vessels that causes significant morbidity and mortality. They also represent a global public health burden and the primary cause of death worldwide. In this research, a novel deep learning-based multi-model image (DL-MMI) has been proposed for detecting CVD. Initially, the input Kaggle datasets images like magnetic resonance imaging (MRI), computed tomography (CT), positron emission tomography (PET), and chest X-ray are fed into wavelet transform-based Multiscale Retinex in the pre-processing phase to enhance the quality of the images. Then the enhanced images are given to GLCM for extracting features in the images. Finally, the dilated convolutional neural network (D-CNN) is used to classify healthy and CVD images. The experimental findings use the specific measures of accuracy, recall, precision, specificity, and F1-score to demonstrate the durability of the DL-MMI approach. Using the Kaggle dataset the proposed DL-MMI method achieves an accuracy rate of 98.89%. The proposed DL-MMI model increases the overall accuracy by 28.62%, 7.51%, and 17.57% than the existing methods such as convolutional auto encoder, CNN, and deep learning, respectively.

This is an open access article under the [CC BY-SA](#) license.



Corresponding Author:

Benila Christabel Thankappan

Department of Computer Science and Research Centre, S.T. Hindu College, Nagercoil - 629002, Affiliated to Manonmaniam Sundaranar University

Abishekapatti, Tirunelveli-627012, Tamilnadu, India

Email: benila.christabel88@gmail.com

1. INTRODUCTION

Heart disease is a group of conditions that affect the heart and blood vessels, often leading to serious health issues like heart attacks and strokes. Blood supply to the heart, brain, and body may be restricted when fat deposits form a blood clot inside an artery, causing the vessel to tighten and constrict [1]. According to predictions, Worldwide, cardiovascular diseases (CVDs) represented 17.9 million deaths in 2019, or 32% of all fatalities [2]. CVDs are the leading cause of mortality worldwide, with 85% of cases attributed to heart attacks and strokes, primarily occurring in low- and middle-income countries [3], [4]. Controlling risk factors can help prevent the majority of cardiovascular diseases related to behavior including obesity, eating disorders, smoking, inactivity, and excessive alcohol consumption [5], [6]. Radiologists can image internal body structures with the aid of diagnostic radiography to identify the origin of symptoms, check for illnesses, and gauge a patient's reaction to treatment [7], [8]. X-rays, Positron emission tomography, ultrasonography, Imaging, basic computed tomography, and magnetic resonance imaging (MRI) are the radiological treatments that are most frequently performed [9], [10]. The fundamental drawback of all gamma-ray and x-ray imaging techniques is the chance that patients will be exposed to radiation [11], [12].

Ultrasonic imaging is helpful since it doesn't radiologists to radiation, or expose patients but the images can be difficult to interpret because it doesn't penetrate well through bone or air [13]. Anatomical changes in tissues can be seen on MRI and computed tomography (CT) scans, while biochemical and physiological changes which frequently take place before morphological changes can be seen on positron emission tomography (PET) scans [14]. Advancements in technology such as surgical robots are revolutionizing the field of diagnostics and treatment [15]. Surgical robots offer precision and control during procedures to enhance the ability to perform complex surgeries with minimal invasiveness. These robots can be integrated with diagnostic imaging tools to provide real-time feedback and assist in the precise targeting of affected areas, thereby improving outcomes for CVD patients [16]. The integration of surgical robots into treatment plans represents a significant advancement in managing cardiovascular diseases, complementing traditional imaging and diagnostic methods [17].

Several studies have explored innovative approaches to cardiovascular disease (CVD) diagnosis and classification. Kumar and Ramana [18] developed a novel method using MRI and severity analysis, establishing the cat fuzzy neural approach for diagnosing conditions including heart attacks, angina, strokes, coronary heart disease, and arrhythmias. Their HAC-ABO technique effectively analyzed damage and segmented affected regions from MRI, achieving an accuracy of 99.3% compared to earlier methods. Ammar *et al.* [19] created an ensemble of classifiers and a deep learning (DL) network for categorizing heart diseases and segmenting cardiac anatomy in cine MRI short-axis images. Their U-Net variant with fewer trainable parameters attained an accuracy of 0.92 for disease categorization and demonstrated good agreement with clinical indices. Velzen *et al.* [20] suggested a technique utilizing chest CT images for lung screening to forecast cardiovascular death, emphasizing the importance of structures like the aorta and coronary arteries in predicting CVD mortality.

Liu *et al.* [21] enhanced low-resolution greyscale PET images with an upgraded Grab Cut segmentation method and improved technique, along with a convolutional neural network, to accurately position and crop the heart in cardiac CT images. Chen *et al.* [22] suggested a DL system for classifying and locating myocardial infarction using a two-stage architecture with stacked denoising autoencoders and an SVM model, focusing on intensity and motion properties in 2D cardiac MRI sequences. Wolterink *et al.* [23] introduced a fully automatic CNN-based technique for segmenting MR images of the myocardial, right ventricle, and left ventricle, achieving 91% multi-class accuracy and 92% accuracy in disease classification. Matsumoto *et al.* [24] suggested a DL algorithm for identifying heart failure from chest X-ray images, which, through data augmentation and transfer learning, achieved 82% accuracy, aiding general practitioners in diagnosing heart failure. Existing methods use a single image to detect CVD disease, but our proposed method uses multiple images to detect CVD disease, and disease severity analysis and classification are critical. The suggested method resolves these problems and correctly categorizes the CVD.

This study proposed DL-MMI has been proposed for detecting CVD. Initially, the input Kaggle datasets images like MRI, CT, PET, and chest X-ray are fed into Wavelet transform-based Multiscale Retinex in the pre-processing phase to enhance the image quality. Then the enhanced images are given to the GLCM for extracting features in the images. Finally, the dilated convolutional neural network is used to categorize healthy and CVD images.

The rest of the paper is structured as follows. In section 2, the proposed methodology is described. Additionally, section 3 gives the findings and analysis of the proposed study. Section 4 explains the work's conclusion.

2. PROPOSED METHODOLOGY

In this section, a novel DL-MMI has been proposed for detecting CVD. The multi-modal images like MRI, CT, PET, and chest X-ray are collected from datasets that are openly accessible. The gathered images undergo pre-processing using Wavelet transform-based Multiscale Retinex to enhance the quality of the images. Then the enhanced images are given to GLCM for extracting features in the images. Finally, the dilated convolutional neural network is utilized to classify healthy and CVD images. The overall workflow of the suggested methodology is shown in Figure 1.

2.1. Pre-processing

The input images are pre-processed utilizing the Wavelet transformer-based Multiscale Retinex to enhance the quality of the images. It is an advanced technique of image enhancement that effectively enhances image details while preserving natural color balance by combining the advantages of wavelet transform with Multiscale Retinex. The illumination reflectance model, on which the wavelet transform method is based, calculates an image's intensity as (1).

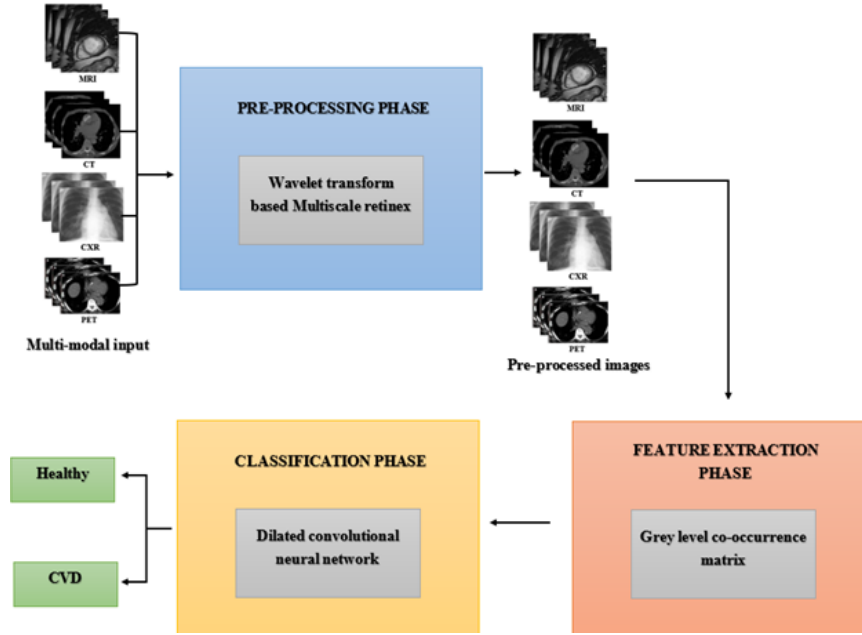


Figure 1. Schematic representation of the proposed DL-MMI framework

$$f(c, d) = u(c, d) v(c, d) \quad (1)$$

Here, $f(c, d)$ stands for the given image, $u(c, d)$ for illumination, and $v(c, d)$ for reflectance. The illumination element is the primary target for elimination. The component of the assembly at the image's edge serves as an explanation for this. There will be high components of the image and low-frequency.

$$\log[f(c, d)] = \log[u(c, d)] + \log[v(c, d)] \quad (2)$$

A data stream is passed through several filters as part of the discrete wavelet transform to produce a set of discrete wavelet coefficients. Convolution is performed by applying filters to apply low-pass and high-pass to the input signal. Several layers of high-frequency coefficients are produced together with a single set of low-frequency coefficients. The Scale Retinex is used to create the Multiscale Retinex as (3),

$$V(a, b) = \log U(a, b) - \log[F(a, b) * U(a, b)] \quad (3)$$

where $V(a, b)$ is the output of Retinex, $F(a, b)$ is the surround function of Gaussian and $v(a, b)$ is the input picture. * Indicates a convolution. Given by, is the Gaussian surround function.

$$F(a, b) = G \cdot e^{-(a^2+b^2)/z^2} \quad (4)$$

where the Gaussian-shaped surrounding constant is denoted by z . The value of z , which is dictated by G and is connected to the visual angle, is selected in such a way that,

$$\iint F(a, b) da db = 1 \quad (5)$$

$$R_{MSRi} = \sum_{m=1}^M \omega_m R_{mi} \quad (6)$$

where M is the scale's number R_{mi} and is the various scales for the Retinex Scale. Each Multiscale Retinex weighs a ω_m .

2.2. Feature extraction

A popular method for extracting features from images is the GLCM which analyses the distances between the brightness of each pixel in a picture to extract textural data. The lesion's textural structures are extracted using the GLCM. A grayscale Nearby values' histogram over an image at a specific offset is called a grey-level cooccurrence matrix. Using the GLCM approach, the distance between pixels was used to calculate the angles between them. Entropy gauges the image's overall content,

$$\text{Entropy} = - \sum_u \sum_v \alpha_{u,v} \log 2 \alpha_{u,v} \quad (7)$$

The distance between pixels is defined and described by correlation as, based on how similar the pixels are.

$$\text{Correlation} = \frac{1}{\omega_x \omega_y} \sum_u \sum_v (u - \sigma_x) (v - \sigma_y) \alpha_{u,v} \quad (8)$$

The definition of inertia, which is used to measure the image contrast is,

$$\text{Inertia} = \sum_u \sum_v (u - v)^2 D_{u,v} \quad (9)$$

The energy-based calculations and visualization of the grey-level distributions are as (10):

$$\text{Energy} = \sum_u \sum_v (D_{u,v})^2 \quad (10)$$

The definition of the image's homogeneity, when the inverse difference is calculated, is (11).

$$\text{Inverse difference} = \sum_u \sum_v \frac{D_{u,v}}{|u-v|} \quad (11)$$

When compared to other DWT Methods, while using the GLCM process to extract an image feature can greatly reduce the image compression time, DWT remains a flexible method for compressing whole films.

2.3. Classification

The input images are classified into CVD and normal instances using the dilated convolutional neural network. A CVD MRI, CT, PET, and chest X-ray volume voxels were each given a class label using a purely convolutional CNN that was trained on the categorization of three orthogonal patches with the voxel as their center. The dilated CNN offer broad receptive fields with a minimal set of trainable parameters. The D-CNN architecture is shown in Figure 2.

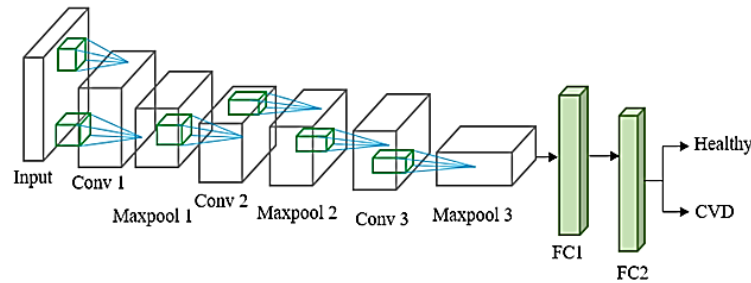


Figure 2. Architecture of D-CNN

CNNs are composed of several convolutional layers that combine at layer $l + 1$, a kernel k and an image F_{l+1} is generated from a layer l 's image F_l . These convolutions are expanded into dilated convolutions, which increase the distance between the kernel's k elements so that adjacent voxels are taken into account while calculating a voxel's value in F_{l+1} . Dilated convolution CNNs have a number of benefits over non-dilated, or conventional, convolution CNNs. A one-dimensional D-CNN that convolves the signal "F" and both of its receptive field sizes ("r") and its dilation ("l"). This can be slightly prolonged to the two-dimensional dilated convolution as (12),

$$(F *_{di} k)_t = \sum_{\tau} k_{\tau} F_{t-di \tau} \quad (12)$$

where $*_{di}$ stands for a dilated convolution of di . Three dilated convolutional layers make up a model, and each layer's dilation factor increases dramatically. The three dilated convolution layers that use the respective dilation convolution (1, 2, 3, 4) and have a particular feature map expressed as (F_1, F_2, F_3, F_4) . For each element in F_{i+1} , the size of the field of receptivity can be viewed as $(2^{i+2} - 1)$.

3. RESULT AND DISCUSSION

This section analyzes the proposed DL-MMI and discusses performance in terms of several assessment criteria. Using libraries and the Python programming language, the recommended structure is created and evaluated on a Windows computer with an Intel Core i7 processor and 16GB of RAM. The efficacy of the proposed approach is assessed using Kaggle datasets [25]. The standards of evaluation employed in this work to examine the efficacy of the proposed strategy include the F1-score, recall, accuracy, precision, and specificity.

The categorization of the proposed DL-MMI approach is illustrated in Figure 3. Column 1 consists of the input images of MRI, CT, PET, and chest X-ray images of CVD. Column 2 shows the enhanced images of CVD. The feature-extracted images of the CVD images are displayed in column 3. Then the classification result of the CVD images is shown in column 4. Finally, the output of the proposed DL-MMI model is displayed in column 5.

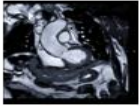

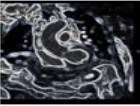
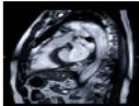
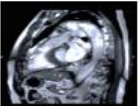

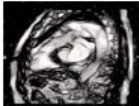

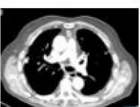
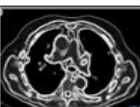



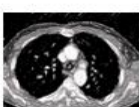
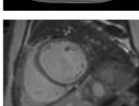
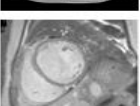
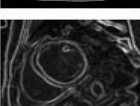
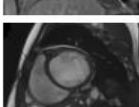
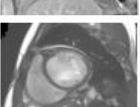
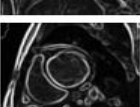
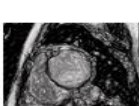
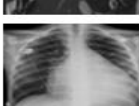
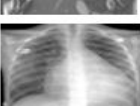
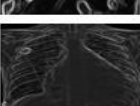


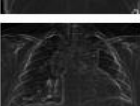

Input	Input images	Pre-processing	Feature extraction	Classification Result	Output
MRI				Healthy	—
				CVD	
CT				Healthy	—
				CVD	
PET				Healthy	—
				CVD	
Chest X-ray				Healthy	—
				CVD	

Figure 3. Classification of two classes in the cardiovascular disease detection (CVD)

3.1. Performance analysis

The following statistical measures are used to evaluate the effectiveness of the classification method: F1 score, accuracy, precision, recall, and specificity. The symbols FP, TP, TF, and FN stand for false-positive, true-positive, true-negative, and false-negative, respectively.

$$Accuracy = \frac{TP+TN}{TP+TN+FP+FN} \quad (16)$$

$$Precision = \frac{TP}{TP+FP} \quad (17)$$

$$Recall = \frac{TP}{TP+TN} \quad (18)$$

$$Specificity = \frac{TN}{TN+FP} \quad (19)$$

$$F1 \text{ score} = 2 \left(\frac{Precision \cdot Recall}{Precision + Recall} \right) \quad (20)$$

Table 1 demonstrates the performance analysis of the DL-MMI method for detecting CVD. It achieves high accuracy with 98.58% for Healthy and 99.21% for CVD. Precision is 96.09% for Healthy and 93.82% for CVD, while specificity is 89.63% and 92.95%, respectively. The recall rates are 96.98% for Healthy and 89.91% for CVD, with F1 scores of 88.99% and 94.29%, respectively. These results indicate that the method effectively distinguishes between healthy individuals and those with CVD.

Table 1. Performance analysis of the suggested method

Classes	Accuracy	Precision	Specificity	Recall	F1 score
Healthy	98.58	96.09	89.63	96.98	88.99
CVD	99.21	93.82	92.95	89.91	94.29

Figure 4 illustrates the performance metrics for two classes, such as healthy and CVD. The suggested technique achieved higher accuracy of 98.58, and 99.21 for healthy and cardiovascular disease. The DL-MMI approach obtains a greater accuracy of 98.89% for the dataset when measured using TPR and FPR parameters. Figure 5(a) shows that the suggested method has realized high accuracy in both validation and training accuracy, and shows loss in Figure 5(b). The suggested model's accuracy of 98.89% meets the performance criteria of accuracy, specificity, and precision.

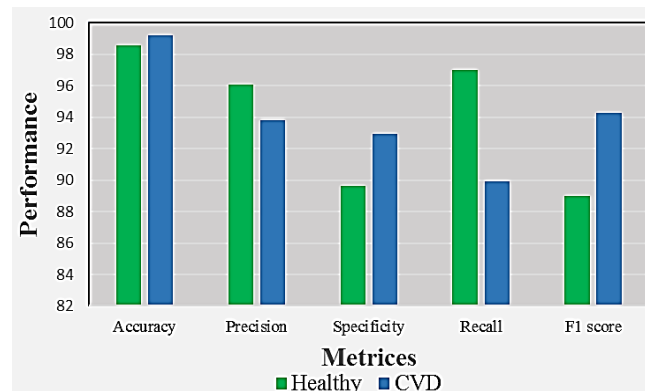


Figure 4. Performance metrics for two classes

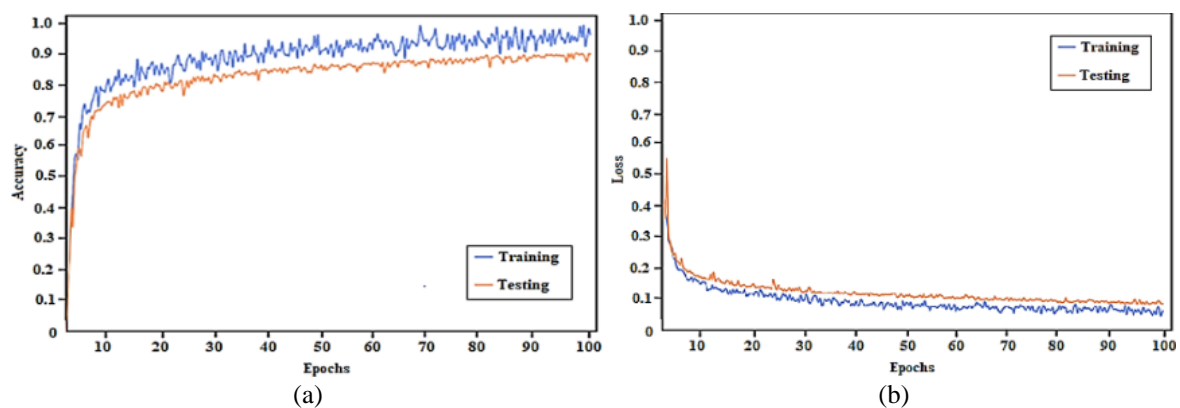


Figure 5. Training and validation (a) accuracy and (b) loss of suggested method

3.2. Comparative analysis

The DL-MMI model is also compared with conventional deep learning networks in this part. This solution performs more productively than existing methodologies when performance is compared. Each of these metrics is used to assess performance: accuracy, precision, and specificity. The proposed method is evaluated with three current DL algorithms in this comparative analysis.

The comparison of various DL networks is shown in Table 2. The suggested D-CNN achieves 96.34% accuracy than Alex Net, DenseNet, and ResNet which obtains 91.09%, 90.21% and 89.90%. Figure 6 illustrates the performance of DL networks Alex Net, Dense Net, and Resnet which attain accuracy of 91.09%, 90.21% and 89.90%, respectively. The D-CNN attains a better accuracy rate than the models that are already in use. A range of criteria were used to estimate each network's performance, including specificity, recall, precision, accuracy, and F1 score.

Table 2. Comparison between traditional DL networks

Networks	Accuracy	Specificity	Precision	Recall	F1 Score
AlexNet	91.09%	93.27%	90.18%	93.58%	93.25%
DenseNet	90.21%	89.18%	92.87%	89.25%	89.37%
ResNet	89.90%	91.76%	90.39%	92.78%	88.91%
D-CNN	96.34%	92.95%	94.14%	94.18%	94.59%

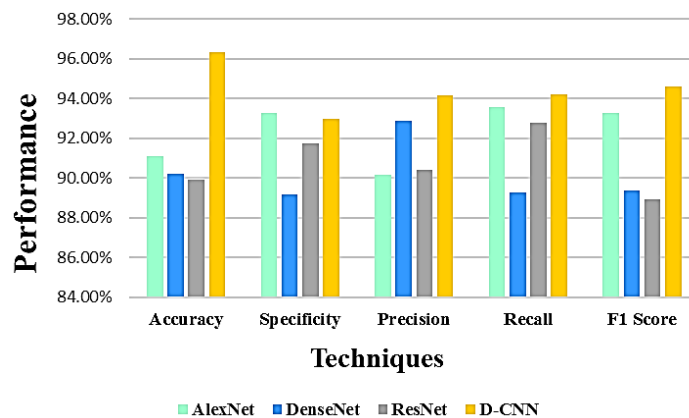


Figure 6. Comparison of traditional DL models

Table 3 shows that the proposed DL-MMI model outperforms convolutional autoencoder, CNN, and deep learning, respectively, in terms of overall accuracy, increasing it by 28.62%, 7.51%, and 17.57%. From the above comparison, the proposed DL-MMI model yields higher accuracy than the existing models.

Table 3. Comparison between the suggested and the existing models

Authors	Approaches	Accuracy
Velzen <i>et al.</i> [20]	Convolutional autoencoder	71%
Wolterink <i>et al.</i> [23]	CNN	92%
Matsumoto <i>et al.</i> [24]	Deep learning	82%
Proposed	DL-MMI	99.48%

3.3. Discussion

In this work, the goal is to detect and categorize the CVD as healthy and CVD using multi-model images. For the experimental analysis, the DL-MMI framework utilizes the Kaggle dataset for the detection of CVD. The results were assessed using accuracy, recall, specificity, precision, and F1-score. Table 1 provides a detailed performance analysis of the proposed method for classifying CVD. The table includes metrics such as precision, specificity, recall, F1 score, and accuracy, for both “Healthy” and “CVD” classes. The method achieves high accuracy, with 98.58% for the Healthy class and 99.21% for the CVD class, indicating robust overall performance. The overall performance metrics of the proposed method such as precision, sensitivity, recall, and f1score attain 94.95%, 91.25%, 93.44%, and 911.64%, respectively.

Figure 5(a) illustrates that the suggested method has attained high accuracy in both training and validation accuracy, and shows low loss in Figure 5(b). The suggested model's accuracy of 98.89% meets the performance criteria of accuracy, specificity, and precision. The comparison of various DL networks is shown in Table 2. The suggested D-CNN achieves 96.34% accuracy than Alex Net, DenseNet, and ResNet which obtains 91.09%, 90.21% and 89.90%. Table 3 shows that the DL-MMI model outperforms the convolutional autoencoder, CNN, and deep learning, respectively, in terms of overall accuracy, increasing it by 28.62%, 7.51%, and 17.57%. The wavelet-based Multiscale Retinex method significantly enhances multimodal medical images by improving contrast and detail preservation, crucial for cardiovascular disease diagnosis. The proposed DL-MMI system achieves a 98.89% accuracy in classifying cardiovascular diseases, outperforming convolutional autoencoder, CNN, and other models by 28.62%, 7.51%, and 17.57%, respectively. Additionally, the D-CNN model demonstrates superior accuracy (96.34%), precision, recall, specificity, and F1-score compared to traditional networks like AlexNet, DenseNet, and ResNet, making it more reliable for cardiovascular disease classification. From this analysis, the DL-MMI approach attains high accuracy with low complexity for detecting CVD in the early stages.

4. CONCLUSION

In this paper, a novel deep learning based multi-model images (DL-MMI) has been proposed for detecting CVD. Initially, the input Kaggle datasets images like MRI, CT, PET and chest X-ray are fed into wavelet transform-based Multiscale Retinex in the pre-processing phase to enhance the quality of the images. Then the enhanced images are fed into GLCM for extracting features in the images. Finally, the D-CNN is utilized to classify healthy and CVD images. The experimental findings use the specific measures of precision, recall, specificity accuracy, and F1-score to demonstrate the durability of the proposed approach. The evidence provided in support of the conclusion is based on a comprehensive evaluation of the proposed system using a range of performance metrics based on the Kaggle dataset. The DL-MMI approach achieves a significantly higher accuracy rate of 98.89% in detecting and classifying cardiovascular disease, outperforming existing methods by 28.62%, 7.51%, and 17.57% compared to Convolutional Autoencoder, CNN, and other deep learning models, respectively. For future work, while our current dataset size is moderate, we plan to expand it to include additional data, which will further enhance the model's accuracy. Additionally, we aim to integrate a surgical robot into our system to provide real-time diagnostic support and assist in the decision-making process during surgical interventions.

ACKNOWLEDGEMENTS

The author would like to express his heartfelt gratitude to the supervisor for his guidance and unwavering support during this research for his guidance and support.





REFERENCES

- [1] O. Gaidai, Y. Cao, and S. Loginov, "Global cardiovascular diseases death rate prediction," *Current Problems in Cardiology*, vol. 48, no. 5, May 2023, doi: 10.1016/j.cpcardiol.2023.101622.
- [2] G. A. Mensah, G. A. Roth, and V. Fuster, "The global burden of cardiovascular diseases and risk factors: 2020 and beyond," *Journal of the American College of Cardiology*, vol. 74, no. 20, pp. 2529–2532, Nov. 2019, doi: 10.1016/j.jacc.2019.10.009.
- [3] M. Walli-Attaei *et al.*, "Variations between women and men in risk factors, treatments, cardiovascular disease incidence, and death in 27 high-income, middle-income, and low-income countries (PURE): a prospective cohort study," *The Lancet*, vol. 396, no. 10244, pp. 97–109, Jul. 2020, doi: 10.1016/S0140-6736(20)30543-2.
- [4] Y. Wang *et al.*, "Activation of the sirutin silent information regulator 1 pathway inhibits pathological myocardial remodeling," *Frontiers in Pharmacology*, vol. 14, Feb. 2023, doi: 10.3389/fphar.2023.1111320.
- [5] A. Khan, R. Uddin, and S. M. S. Islam, "Clustering patterns of behavioural risk factors for cardiovascular diseases in Bangladeshi adolescents: A population-based study," *Health Policy and Technology*, vol. 8, no. 4, pp. 386–392, Dec. 2019, doi: 10.1016/j.hlpt.2019.09.003.
- [6] S. Aggarwal and K. Pandey, "Early identification of PCOS with commonly known diseases: Obesity, diabetes, high blood pressure and heart disease using machine learning techniques," *Expert Systems with Applications*, vol. 217, May 2023, doi: 10.1016/j.eswa.2023.119532.
- [7] P. O. Samuel *et al.*, "Lifestyle modifications for preventing and managing cardiovascular diseases," *Sport Sciences for Health*, vol. 20, no. 1, pp. 23–36, Aug. 2024, doi: 10.1007/s11332-023-01118-z.
- [8] Z. Zhang and E. Sejdić, "Radiological images and machine learning: trends, perspectives, and prospects," *Computers in Biology and Medicine*, vol. 108, pp. 354–370, May 2019, doi: 10.1016/j.compbiomed.2019.02.017.
- [9] O. G. Duliu, "X- and gamma ray imaging (CT, PET and SPEC, scintigraphy, and radiography): benefits and risks," in *Medical Imaging Methods: Theory and Applications*, CRC Press, 2021, pp. 57–90.
- [10] A. Komaraju and A. Chhabra, "Advanced cross-sectional radiology-ultrasound, computed tomography and magnetic resonance imaging of the diabetic foot," *The Foot in Diabetes*. Wiley, pp. 169–185, Apr. 2020, doi: 10.1002/9781119445821.ch10.
- [11] B. Martins, D. Ferreira, C. Neto, A. Abelha, and J. Machado, "Data mining for cardiovascular disease prediction," *Journal of Medical Systems*, vol. 45, no. 1, Jan. 2021, doi: 10.1007/s10916-020-01682-8.
- [12] Y. D. Zhang *et al.*, "Advances in multimodal data fusion in neuroimaging: Overview, challenges, and novel orientation,"




- Information Fusion*, vol. 64, pp. 149–187, Dec. 2020, doi: 10.1016/j.inffus.2020.07.006.
- [13] C. Krittanawong *et al.*, “Machine learning prediction in cardiovascular diseases: a meta-analysis,” *Scientific Reports*, vol. 10, no. 1, Sep. 2020, doi: 10.1038/s41598-020-72685-1.
- [14] S. N. Pasha, D. Ramesh, S. Mohmmad, A. Harshavardhan, and Shabana, “Cardiovascular disease prediction using deep learning techniques,” *IOP Conference Series: Materials Science and Engineering*, vol. 981, no. 2, Dec. 2020, doi: 10.1088/1757-899X/981/2/022006.
- [15] K. Szymańska *et al.*, “Revolutionizing cardiovascular treatments with the use of AI: Current status and future prospects,” *Quality in Sport*, vol. 19, Jul. 2024, doi: 10.12775/qs.2024.19.53072.
- [16] J. Bonatti, G. Vetrovec, C. Riga, O. Wazni, and P. Stadler, “Robotic technology in cardiovascular medicine,” *Nature Reviews Cardiology*, vol. 11, no. 5, pp. 266–275, Mar. 2014, doi: 10.1038/nrcardio.2014.23.
- [17] R. H. Taylor, A. Menciassi, G. Fichtinger, P. Fiorini, and P. Dario, “Medical robotics and computer-integrated surgery,” in *Springer Handbooks*, Springer International Publishing, 2016, pp. 1657–1684.
- [18] M. D. Kumar and K. V. Ramana, “Cardiovascular disease prognosis and severity analysis using hybrid heuristic methods,” *Multimedia Tools and Applications*, vol. 80, no. 5, pp. 7939–7965, Oct. 2021, doi: 10.1007/s11042-020-10000-w.
- [19] A. Ammar, O. Bouattane, and M. Youssfi, “Automatic cardiac cine MRI segmentation and heart disease classification,” *Computerized Medical Imaging and Graphics*, vol. 88, Mar. 2021, doi: 10.1016/j.compmedimag.2021.101864.
- [20] S. van Velzen *et al.*, “Direct prediction of cardiovascular mortality from low-dose chest CT using deep learning,” in *Medical Imaging 2019: Image Processing*, Mar. 2019, doi: 10.1117/12.2512400.
- [21] H. Liu, W. Chu, and H. Wang, “Automatic segmentation algorithm of ultrasound heart image based on convolutional neural network and image saliency,” *IEEE Access*, vol. 8, pp. 104445–104457, 2020, doi: 10.1109/ACCESS.2020.2989819.
- [22] M. Chen, L. Fang, Q. Zhuang, and H. Liu, “Deep learning assessment of myocardial infarction from MR image sequences,” *IEEE Access*, vol. 7, pp. 5438–5446, 2019, doi: 10.1109/ACCESS.2018.2889744.
- [23] J. M. Wolterink, T. Leiner, M. A. Viergever, and I. Išgum, “Automatic segmentation and disease classification using cardiac cine MR images,” in *Lecture Notes in Computer Science (including subseries Lecture Notes in Artificial Intelligence and Lecture Notes in Bioinformatics)*, vol. 10663 LNCS, Springer International Publishing, 2018, pp. 101–110.
- [24] T. Matsumoto *et al.*, “Diagnosing heart failure from chest X-ray images using deep learning,” *International Heart Journal*, vol. 61, no. 4, pp. 781–786, Jul. 2020, doi: 10.1536/ihj.19-714.
- [25] L. Quaranta, F. Calefato, and F. Lanubile, “KGTorrent: a dataset of python Jupyter notebooks from Kaggle,” in *Proceedings - 2021 IEEE/ACM 18th International Conference on Mining Software Repositories, MSR 2021*, May 2021, pp. 550–554, doi: 10.1109/MSR52588.2021.00072.

BIOGRAPHIES OF AUTHORS



Benila Christabel Thankappan    , a research scholar (Register Number: 22223152292015), has been an assistant professor at Women's Christian College, Nagercoil, since 12-08-2013. She is presently pursuing a Ph.D. in computer applications and working in the Computer Science Department. She can be contacted at benila.christabel88@gmail.com or benila456t@outlook.com.



Thanammal Kakkumperumal Krishnammal    (Assistant Professor) received the M.Sc. (Computer Science) degree from Bharathidasan University, Tiruchirappalli in 1992, M.Phil. (Computer Science) degree from Manonmaniam Sundaranar University, Tirunelveli in 1999, M. Tech (Computer Science) Degree from Vinayaka Mission University, Salem in 2007, and Ph.D. (Computer Science) Degree from Manonmaniam Sundaranar University, Tirunelveli in 2015. She has been working as an associate professor in the Computer Science Department at S.T. Hindu College, Nagercoil since 1993. She can be contacted at thanaravindran@gmail.com or thanmmal23567kk@outlook.com.